



Title	Hopping conduction and piezoelectricity in Fe-doped GaN studied by non-contacting resonant ultrasound spectroscopy
Author(s)	Ogi, H.; Tsutsui, Y.; Nakamura, N. et al.
Citation	Applied Physics Letters. 2015, 106(9), p. 091901-1-091901-4
Version Type	VoR
URL	https://hdl.handle.net/11094/83927
rights	Copyright 2015 AIP Publishing LLC. This article may be downloaded for personal use only. Any other use requires prior permission of the author and AIP Publishing. This article appeared in Applied Physics Letters, 106(9), 091901, 2015 and may be found at https://doi.org/10.1063/1.4913973 .
Note	

The University of Osaka Institutional Knowledge Archive : OUKA

<https://ir.library.osaka-u.ac.jp/>

The University of Osaka

Hopping conduction and piezoelectricity in Fe-doped GaN studied by non-contacting resonant ultrasound spectroscopy

Cite as: Appl. Phys. Lett. **106**, 091901 (2015); <https://doi.org/10.1063/1.4913973>

Submitted: 05 January 2015 . Accepted: 20 February 2015 . Published Online: 02 March 2015

H. Ogi,  Y. Tsutsui, N. Nakamura, A. Nagakubo, M. Hirao, M. Imade, M. Yoshimura, Y. Mori, et al.



View Online



Export Citation



CrossMark

ARTICLES YOU MAY BE INTERESTED IN

[Piezoelectric coefficients of GaN determined by hopping conduction of carriers](#)

Applied Physics Letters **109**, 182108 (2016); <https://doi.org/10.1063/1.4966995>

[Elastic constants of GaN between 10 and 305K](#)

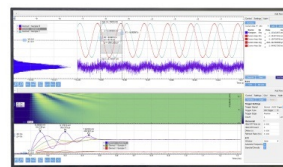
Journal of Applied Physics **119**, 245111 (2016); <https://doi.org/10.1063/1.4955046>

[Unusual elasticity of monoclinic \$\beta\$ -Ga₂O₃](#)

Journal of Applied Physics **124**, 085102 (2018); <https://doi.org/10.1063/1.5047017>

Challenge us.

What are your needs for
periodic signal detection?



Zurich
Instruments



Hopping conduction and piezoelectricity in Fe-doped GaN studied by non-contacting resonant ultrasound spectroscopy

H. Ogi,^{1,a)} Y. Tsutsui,¹ N. Nakamura,¹ A. Nagakubo,¹ M. Hirao,¹ M. Imade,² M. Yoshimura,² and Y. Mori²

¹Graduate School of Engineering Science, Osaka University, Toyonaka, Osaka 560-8531, Japan

²Graduate School of Engineering, Osaka University, Suita, Osaka 565-0871, Japan

(Received 5 January 2015; accepted 20 February 2015; published online 2 March 2015)

Using the antenna-transmission acoustic-resonance technique, we measured temperature dependencies of mechanical resonance frequencies and attenuation of an Fe-doped GaN. A strong internal-friction peak appears during temperature change, at which reduction in frequency occurs. The peak temperature rises as frequency increases, indicating the phonon-assisted hopping conduction of carriers between Fe centers. The Arrhenius plot yields the activation energy of the hopping conduction to be 0.23 ± 0.05 eV. The frequency reduction of a quasi-plane-shear resonance mode yields the piezoelectric coefficient $e_{15} = 0.332 \pm 0.03$ C/m². © 2015 AIP Publishing LLC.

[<http://dx.doi.org/10.1063/1.4913973>]

Fe ions have been doped in gallium nitride (GaN) as deep acceptors for compensating n-type carriers to achieve a semi-insulating GaN,^{1–4} which is a key material in various electric devices such as a high-electron-mobility transistor (HEMT).^{1,5–7} The device performances, however, deteriorate with increasing temperature.^{8–10} Deeply trapped carriers in the bulk GaN can be thermally activated, causing the hopping conduction,^{11,12} which creates the additional electron pass and affects the carrier mobility.⁸ It is thus important to understand electron transport behavior at elevated temperatures in the semi-insulating GaN.

Equally important issue is the piezoelectricity of GaN. Wurtzite GaN shows five independent elastic constants C_{ij} and three independent piezoelectric coefficients e_{ij} (e_{33} , e_{31} , and e_{15}). A complete set of C_{ij} was determined with resonant ultrasound spectroscopy (RUS)¹³ for bulk GaN specimens, where e_{ij} were deduced as well, but they were significantly underestimated because of high carrier densities of the specimens. A few theoretical^{14–17} and experimental¹⁸ studies gave e_{33} and e_{31} values, but they significantly differ from each other. (The standard deviation of reported values of e_{33} exceeds 20% of their averaged value, for example.) Furthermore, few theoretical reports¹⁶ and no direct measurement appear for e_{15} , the piezoelectric coefficient related to the shear stress. Thus, the piezoelectricity of GaN still remains unclear despite its crucial contribution to the two-dimensional electron gas in HEMT devices. Simultaneous determination of C_{ij} and e_{ij} has been proven to be possible with the RUS method.^{19,20} However, it required extraordinarily precise measurements on resonant frequencies, specimen dimensions, and specimen mass density because of small contributions of e_{ij} to frequencies,¹⁹ and is therefore inapplicable to GaN because contributions of e_{ij} are considerably smaller due to high stiffness.

In this study, we propose a methodology for evaluating the carrier dynamics and piezoelectricity in Fe-doped GaN with the antenna-transmission resonant ultrasound

spectroscopy and determine the activation energy of the hopping conduction and the piezoelectric coefficient e_{15} . The free-carrier flow is restricted in an insulated semiconductor, and the conduction principally occurs by hopping of trapped carriers by acceptors between the sites. The hopping conduction is a thermally activated phenomenon; the phonon-assisted carrier movement is efficiently enhanced when the polarization-switching rate caused by ultrasonic vibration is matched with the jump rate of a carrier from site to site. Thus, focusing a resonant mode, internal friction shows a maximum with increasing temperature because a part of the acoustic energy is spent on the carrier movement, and the frequency decrement (modulus defect) occurs at the matching temperature.²¹ The resonance-frequency change Δf and corresponding attenuation coefficient α take the Debye-type relaxation forms^{21,22}

$$\frac{\Delta f}{f} = \frac{e^2}{2C\epsilon} \times \frac{(\omega\tau)^2}{1 + (\omega\tau)^2}, \quad (1)$$

$$\alpha = \frac{e^2}{2C\epsilon} \times \frac{\omega^2\tau}{1 + (\omega\tau)^2}. \quad (2)$$

Here, ω is the angular frequency, and e , C , and ϵ denote the effective piezoelectric, elastic, and dielectric constants dominating the resonant mode. τ denotes the relaxation time for the carrier hopping expressed by $\tau = \epsilon\rho$ with the resistivity ρ . The attenuation coefficient thus shows a peak at $\omega\tau = 1$, across which the modulus defect appears. Because the resistivity is inversely proportional to the Boltzmann factor ($\rho \propto \exp(E/kT)$),¹¹ an Arrhenius plot for the peak attenuation yields the activation energy E . The resonance-frequency shift across the attenuation peak reflects the disappearance of the apparent piezoelectricity due to the hopping conduction, and it is possible to determine the piezoelectric coefficient by measuring the frequency shift. This approach determines the piezoelectric coefficient much more accurately than the conventional methods because the frequency shift can be accurately measured by monitoring the relative frequency change. (Note that the previous

^{a)}ogi@me.es.osaka-u.ac.jp

method requires absolute measurements for frequencies with extraordinary precision.)

The material we used was grown with a hydride-vapour-phase-epitaxy (HVPE) method. Because the HVPE method introduces many donors mainly from silicon and oxygen,²³ Fe ions were introduced to compensate them.^{3,24} The resistivity at room temperature and Fe concentration are $2 \times 10^8 \Omega \text{ cm}$ and $8 \times 10^{18} \text{ cm}^{-3}$, respectively. The mass density determined by the Archimedes method is 6.080 g/cm^3 . The GaN wafer was machined to obtain a rectangular-parallelepiped specimen with $3.493 \times 2.990 \times 0.410 \text{ mm}^3$. (The c axis is along the thickness direction.)

The antenna-transmission technique^{25,26} was used for causing free vibrations of the thin GaN specimen contactlessly through the piezoelectric coupling with dynamic electric fields. Two line-antenna configurations were developed as illustrated in Figs. 1(a) and 1(b) for multimode and single mode excitations, respectively. The former causes the dynamic electric field along inclined directions to the surface, exciting various vibrational modes as shown in Fig. 1(c), while the latter principally causes the electric fields parallel to the surface, which is coupled into the shear deformation through e_{15} , giving rise to the shear vibration strongly as shown in Fig. 1(d). The specimen and antenna were set inside a tube heater located in a vacuum chamber, where the pressure during the experiments was kept under $\sim 1 \times 10^{-2} \text{ Pa}$. Details of the high-temperature non-contacting RUS system appear elsewhere.²⁶ The attenuation coefficients were measured from the ring-down signals after excitation with tone bursts.²⁷ The acoustically contactless measurement is the key for the accurate attenuation measurement, because any contacts to the specimen cause energy leakage, leading to significantly larger apparent attenuation.²⁷

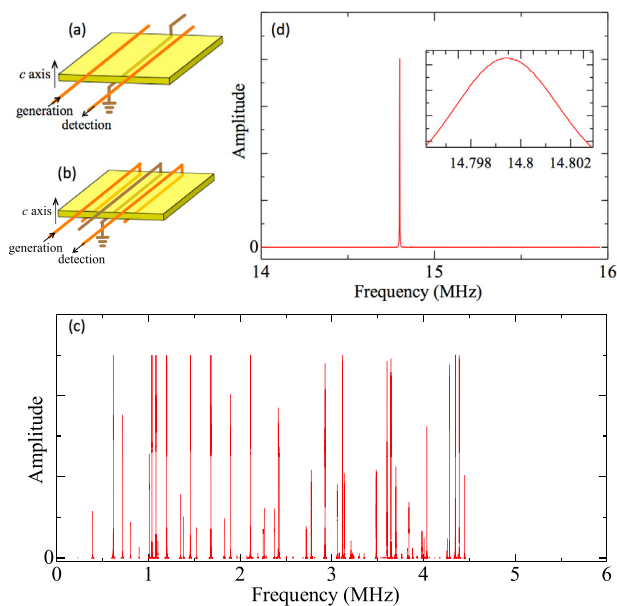


FIG. 1. (a) Antenna configuration for multimode excitation and (b) that for shear mode excitation. (c) Resonant spectrum measured by the multimode antennas and (d) that by the shear-mode antennas. The inset enlarges the measurement near the single peak.

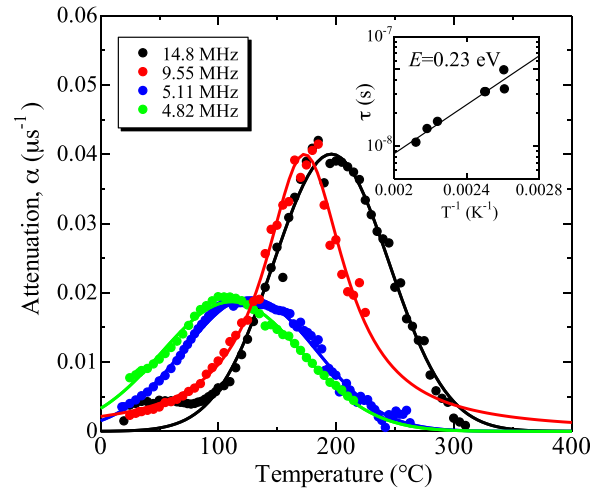


FIG. 2. Temperature dependence of the attenuation coefficient with various frequencies. The inset shows the Arrhenius plot, yielding the activation energy.

Figure 2 shows temperature behavior of the attenuation coefficient for various resonance modes. The attenuation-peak temperature rises as the frequency increases, and the Arrhenius plot yields the activation energy of $0.23 \pm 0.05 \text{ eV}$. Previous studies used optical spectroscopy methods for studying excited states of Fe ions in GaN,^{24,28} where the formation of an Fe^{2+} -hole complex was suggested and their binding energy was estimated. However, various energy bands were superimposed in their spectra, and it was fairly difficult to identify the energy states with the phonon-assisted charge transfer process from such broad spectra. For example, Heitz *et al.*²⁸ estimated the binding energy for the complex to be 0.28 eV , whereas Malguth *et al.*²⁴ denied this value and presented a much smaller value of 0.05 eV . Thus, the lower energy bands of the charge transfer processes coupled with phonons have not been clearly observed. In contrast, our acoustic-resonance method allows the direct excitation of the phonon-assisted carrier flow and then unambiguous determination of the activation energy. Our value, 0.23 eV , is closer to that estimated by Heitz *et al.*

Also challenging subject is determination of the piezoelectric coefficient, especially e_{15} . Cooling from high enough temperature increases the relaxation time for hopping of carriers and they eventually fail to follow the polarization change caused by acoustic vibration at temperatures below enough the attenuation-peak temperature. This causes an increase in the resonant frequency, corresponding to the piezoelectric stiffening. Thus, the frequency shift reflects the piezoelectric coefficient, which can be determined by measuring the frequency shift. Although many resonant peaks are observed with the antenna configuration in Fig. 1(a), most of them disappear at elevated temperatures beyond the attenuation peak due to disappearing of piezoelectricity, and we failed to measure the frequency changes accurately. However, we find that the nearly pure shear-resonance mode is observable even at temperatures beyond the attenuation peak as shown in Fig. 3: The antenna configuration in Fig. 1(b) causes the in-plane dynamic electric field, which selectively excites and detects the shear vibrations through the coupling with e_{15} , making the single resonance peak

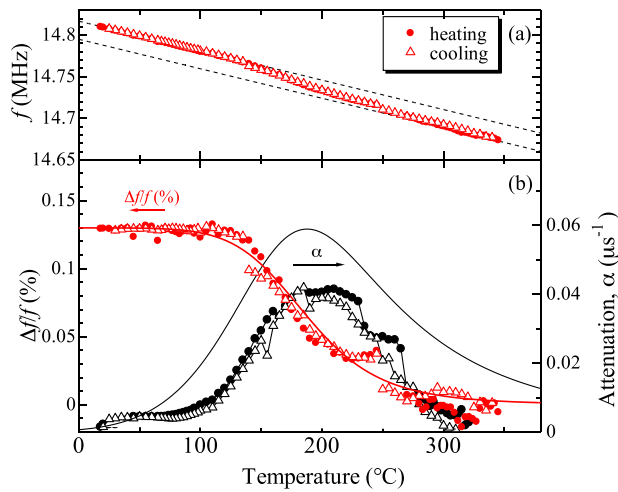


FIG. 3. (a) The resonance-frequency change with temperature for the shear vibration mode. The broken lines indicate temperature dependences of the frequency at low and high temperature regions. (b) The baseline-subtracted fractional frequency change and the attenuation-coefficient change during heating and cooling processes. The solid lines are theories in Eqs. (1) and (2), where the parameters were determined by fitting them to the frequency change.

observable at 14.8 MHz (Fig. 1(d)), which is nearly identical to the third through-thickness shear-wave resonance. (Using the reported shear modulus $C_{44} = 98.0$ GPa,¹³ the third through-thickness shear-wave resonance frequency is calculated to be 14.7 MHz.) The frequency shift and corresponding attenuation peak are clearly observed for this mode as shown in Fig. 3, where theoretical calculations based on Eqs. (1) and (2) are shown with solid lines. The frequency and attenuation behaviors were identical between the heating and cooling processes, indicating the thermally activated relaxation phenomenon. Note that, however, the piezoelectric stiffening does not occur for the pure shear plane wave propagating along the c -axis, and the shear free vibration at 14.8 MHz is not the same as the plane-wave resonance mode. Therefore, exact mode identification and precise calculation of the e_{15} contribution to this mode are necessary.

We computed free-vibration resonance frequencies using the Ritz method with basis functions composed of the Legendre-polynomial products^{19,29} $\hat{P}_l(x_1/L_1)\hat{P}_m(x_2/L_2)\hat{P}_n(x_3/L_3)$, where \hat{P} represents the normalized Legendre function, and x_1 , x_2 , and x_3 are the Cartesian coordinates along the rectangular-parallelepiped edges (along 3.493-mm, 2.990-mm, and 0.410-mm edges), respectively. L_i denotes the edge length along the x_i axis of the specimen. l , m , and n denote the order numbers of the Legendre polynomial ($l + m + n \leq N$). For calculating the resonance frequencies at higher modes, we need to involve sufficiently higher-order Legendre polynomials. Figure 4 displays differences of computed resonance frequencies from those using Legendre polynomials up to $N = 70$, in which more than 7800 basis functions are involved in the computation for each vibration group. (There are eight vibrational groups in an oriented GaN rectangular parallelepiped, depending on the symmetry of deformation and electric potential.²⁹) The resonance frequencies converge to the true values with increasing the number of basis functions, and the difference from the true values will be smaller than 0.001% with $N = 70$ even for frequencies near 15 MHz. We thus involved about

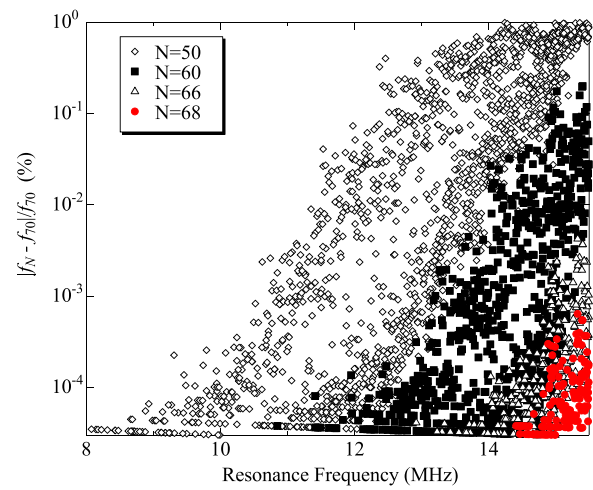


FIG. 4. Differences of resonance frequencies computed by the Ritz method with various N values. N denotes the maximum order number of Legendre polynomial in basis functions, and the differences are relative to frequencies with $N = 70$.

7800 basis functions with $N = 70$ for calculating the piezoelectric coefficient.

Among the eight vibrational groups, B_{2g} and B_{3g} groups are candidates for the 14.8 MHz resonance mode, because they show the identical deformation symmetry to the through-thickness shear-wave resonance modes. We then identified the 14.8 MHz mode to be 273th overtone of the B_{3g} vibrational group because of three reasons. First, its computed frequency (14.83 MHz) is close to the measurement at room temperature (14.81 MHz). Second, it is highly affected by the shear modulus C_{44} (contribution of C_{44} exceeds 80%), being similar to the through-thickness shear modes. Third, it shows similar displacement distribution to that of the third through-thickness shear resonance as shown in the inset in Fig. 5: The shear displacement along the x_2 axis shows nearly uniform distributions in x_1 - x_2 planes, and it shows the odd symmetry along the thickness direction, which coincides with the oppositely excited tangential

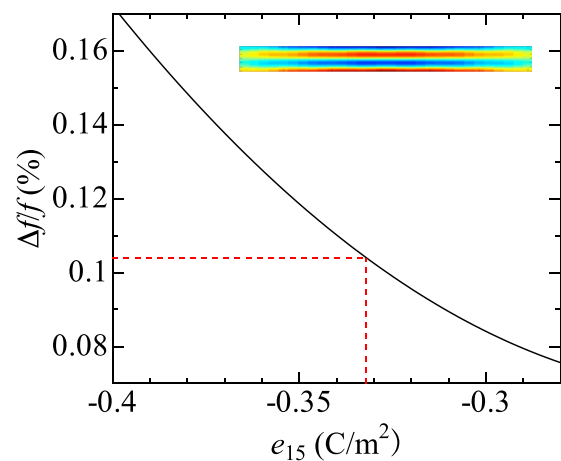


FIG. 5. The sensitivity of the piezoelectric coefficient e_{15} to the quasi shear resonance frequency at 14.8 MHz. The horizontal broken red line indicates the measured frequency change. The inset shows the computed distribution of the shear displacement on the cross-section of the specimen, where red and blue indicate high amplitude regions, but their directions are opposite to each other.

electric fields on both surfaces. We calculated the contributions of the three piezoelectric coefficients to the B_{3g} -273 mode and found that e_{15} was dominant compared with the other two coefficients: Contributions of e_{33} and e_{13} are smaller than that of e_{15} by factors of 0.1. Therefore, we independently calculated the sensitivity of e_{15} to the frequency as shown in Fig. 5: We calculated the frequency shift from the non-piezoelectric state ($e_{ij} = 0$) by varying e_{15} and compared it with the measurement to determine e_{15} . In this calculation, we used C_{ij} values from our previous measurements¹³ and reported dielectric constants $\epsilon_{11}/\epsilon_0 = 5.35$ ³⁰ and $\epsilon_{33}/\epsilon_0 = 5.80$.³¹ (We also involved reported piezoelectric constants e_{33} and e_{13} ,¹⁶ but they are not sensitive to the resultant e_{15} as mentioned above.) Our measurements provided the frequency shift of $0.104 \pm 0.03\%$, yielding $e_{15} = -0.332 \pm 0.03 \text{ C/m}^2$. The absolute value is smaller than that of the reported theoretical value (-0.38 C/m^2)¹⁶ by 14%.

In summary, we have acoustically measured the activation energy of carrier's hopping conduction in Fe-doped GaN. The temperature dependence of the relaxation time was evaluated through the vibration-attenuation peak, and the Arrhenius plot yielded the activation energy to be $0.23 \pm 0.05 \text{ eV}$. The piezoelectric coefficient e_{15} related to the shear deformation was then determined by the frequency decrement for the quasi shear resonance mode caused by disappearance of piezoelectricity due to the hopping conduction. Because there is no measurement and only one theoretical report on e_{15} , our measurement value $e_{15} = -0.332 \pm 0.03 \text{ C/m}^2$ is crucially important.

¹B. Monemar and O. Lagerstedt, *J. Appl. Phys.* **50**, 6480 (1979).

²K. Maier, M. Kunzer, U. Kaufmann, J. Schneider, B. Monemar, I. Akasaki, and H. Amano, *Mater. Sci. Forum* **143–147**, 93 (1994).

³S. Heikman, S. Keller, S. P. DenBaars, and U. K. Mishra, *Appl. Phys. Lett.* **81**, 439 (2002).

⁴M. Kubota, T. Onuma, Y. Ishihara, A. Usui, A. Uedono, and S. F. Chichibu, *J. Appl. Phys.* **105**, 083542 (2009).

⁵R. P. Vaudo, X. Xu, A. Salant, J. Malcarne, and G. R. Brandes, *Phys. Status Solidi A* **200**, 18 (2003).

⁶J. R. Shealy, V. Kaper, V. Tilak, T. Prunty, J. A. Smart, B. Green, and L. F. Eastman, *J. Phys.: Condens. Matter* **14**, 3499 (2002).

⁷S. Arulkumaran, T. Egawa, H. Ishikawa, T. Jimbo, and Y. Sano, *Appl. Phys. Lett.* **84**, 613 (2004).

⁸O. Aktas, Z. F. Fan, S. N. Mohammad, A. E. Botchkarev, and H. Morkoç, *Appl. Phys. Lett.* **69**, 3872 (1996).

⁹N. Maeda, K. Tsubaki, T. Saitoh, and N. Kobayashi, *Appl. Phys. Lett.* **79**, 1634 (2001).

¹⁰K. Tanaka, M. Ishida, T. Ueda, and T. Tanaka, *Jpn. J. Appl. Phys., Part 1* **52**, 04CF07 (2013).

¹¹F. Mott and W. D. Twose, *Adv. Phys.* **10**, 107 (1961).

¹²D. C. Look, D. C. Reynolds, W. Kim, Ö. Aktas, A. Botchkarev, A. Salvador, and H. Morkoç, *J. Appl. Phys.* **80**, 2960 (1996).

¹³N. Nakamura, H. Ogi, and M. Hirao, *J. Appl. Phys.* **111**, 013509 (2012).

¹⁴F. Bernardini, V. Fiorentini, and D. Vanderbilt, *Phys. Rev. B* **56**, R10024 (1997).

¹⁵A. Zorodu, F. Bernardini, and P. Ruggerone, *Phys. Rev. B* **64**, 045208 (2001).

¹⁶K. Shimada, *Jpn. J. Appl. Phys., Part 2* **45**, L358 (2006).

¹⁷Y. Duan, J. Li, S. Li, and J. Xia, *J. Appl. Phys.* **103**, 023705 (2008).

¹⁸I. L. Guy, S. Muensit, and E. M. Goldys, *Appl. Phys. Lett.* **75**, 4133 (1999).

¹⁹H. Ogi, T. Ohmori, N. Nakamura, and M. Hirao, *J. Appl. Phys.* **100**, 053511 (2006).

²⁰H. Ogi, N. Nakamura, K. Sato, M. Hirao, and S. Uda, *IEEE Trans. Ultrason. Ferroelectr. Freq. Control* **50**, 553 (2003).

²¹A. R. Hutson and D. L. White, *J. Appl. Phys.* **33**, 40 (1962).

²²P. Debye, *Polar Molecules* (Dover Publications, Inc., New York, 1929), p. 93.

²³G. Pozina, S. Khromov, C. Hemmingsson, L. Hultman, and B. Monemar, *Phys. Rev. B* **84**, 165213 (2011).

²⁴E. Malmuth, A. Hoffmann, W. Gehlhoff, O. Gelhausen, M. R. Phillips, and X. Xu, *Phys. Rev. B* **74**, 165202 (2006).

²⁵H. Ogi, H. Niho, and M. Hirao, *Appl. Phys. Lett.* **88**, 141110 (2006).

²⁶N. Nakamura, M. Sakamoto, H. Ogi, and M. Hirao, *Rev. Sci. Instrum.* **83**, 073901 (2012).

²⁷H. Ogi, H. Ledbetter, S. Kim, and M. Hirao, *J. Acoust. Soc. Am.* **106**, 660 (1999).

²⁸R. Heitz, P. Maxim, L. Eckey, P. Thurian, A. Hoffmann, I. Broser, K. Pressel, and B. K. Meyer, *Phys. Rev. B* **55**, 4382 (1997).

²⁹I. Ohno, *Phys. Chem. Miner.* **17**, 371 (1990).

³⁰A. S. Barker, Jr. and M. Ilegems, *Phys. Rev. B* **7**, 743 (1973).

³¹D. D. Manchon, Jr., A. S. Barker, Jr., P. J. Dean, and R. B. Zetterstrom, *Solid State Commun.* **8**, 1227 (1970).